Journal of Magnetic Resonance **146,** 43–48 (2000)
doi:10.1006/jmre.2000.2146, available online at http://www.idealibrary.com on IDEAL®

The Nutation Spin Echo and Its Use for Localized NMR

Ioan Ardelean,[1] Rainer Kimmich, and Andreas Klemm

Sektion Kernresonanzspektroskopie, Universität Ulm, 89069 Ulm, Germany

Received October 14, 1999; revised June 16, 2000

A suitably matched combination of unidirectional gradient pulses of the radio frequency amplitude B_1 and of the main magnetic field B_0 produces an unconventional type of spin echo, the nutation echo. The echo signal becomes volume selective if the gradients to be matched are inhomogeneously distributed in space. An example is a combination of a constant B_0 gradient and the inhomogeneous B_1 gradient of a surface coil. We suggest a method for localized NMR on this basis. Nutation echoes can also be used to map the spatial distribution of B_1 gradients of an arbitrary radio frequency coil geometry with the aid of a small probe sample. © 2000 Academic Press

Key Words: **nutation; spin echo; volume selection; localized spectroscopy; B_1 gradients.**

1. INTRODUCTION

In Refs. (*1–5*) spin-echo phenomena are reported based on coherence evolution in a combination of gradients of the external magnetic field B_0 and of the radio frequency (RF) amplitude B_1. In the treatment published in Ref. (*4*) the nature of the so-called "nutation echo" (and of higher order multiple nutation echoes) was given. In the present study we concentrate on the nutation echo which by nature is analogous to the ordinary Hahn echo. It is produced by a pulse subject to a gradient of the RF amplitude $B_{1\perp}$ (component perpendicular to the external magnetic field $\mathbf{B_0}$) if it is followed by a suitably matched B_0 gradient pulse. The nutation echo is of particular interest for potential applications because it is expected to have the same signal strength as the ordinary Hahn echo produced by a pulse sequence $\pi/2$–τ–$\pi/2$–τ in the presence of a B_0 gradient. In the following we will point out that the nutation echo can be used as a tool suitable for localized spectroscopy, relaxation, diffusion, or flow measurements.

The nutation echo is not to be confused with higher order multiple nutation echoes reported in Refs. (*3, 4*). These "nonlinear" echoes arise only if demagnetizing field effects play a role in complete analogy to the laboratory-frame multiple echoes (*6–9*). Just like the ordinary Hahn echo, the "linear" nutation echo to be considered here appears even if the demagnetizing field is negligible. This in particular occurs if the external magnetic field is low.

2. THEORETICAL CONSIDERATIONS

The basic pulse sequence used for producing the nutation echo is schematically shown in Fig. 1. Note that the $B_{1\perp}$ and B_0 gradients, $\mathbf{G_1}$ and $\mathbf{G_0}$, respectively, need not be constant in the sample volume. In the following we rather consider local gradients existing in a certain volume element centered at a position $\tilde{\mathbf{r}}$. The signal to be expected is proportional to the complex transverse rotating-frame magnetization given as the $l = 1$ term in Eq. 29 of Ref. (*4*). That is

$$m(\tau_1 + \tau_2) = \frac{M_0}{\xi}\, e^{-i\psi} e^{i\alpha} J_1(\xi), \qquad [1]$$

where M_0 is the (local) equilibrium magnetization, and

$$\xi = \gamma_n \mu_0 M_0 \tau_2, \qquad [2]$$

$$\psi = \gamma_n \tau_2 \int_0^{\tilde{\mathbf{r}}} \mathbf{G_0} \cdot \mathrm{d}\tilde{\mathbf{r}}', \qquad [3]$$

$$\alpha = \gamma_n \tau_1 \int_0^{\tilde{\mathbf{r}}} \mathbf{G_1} \cdot \mathrm{d}\tilde{\mathbf{r}}'. \qquad [4]$$

The phase shifts α and ψ acquired in the intervals τ_1 and τ_2, respectively, are defined in such a way that they take the value 0 at the origin. $J_1(\xi)$ is the first-order Bessel function. Note that it can be approximated by $J_1(\xi) \cong \xi/2$ in the limit $\xi \ll 1$. The gyromagnetic ratio is denoted by γ_n, the magnetic field constant by μ_0. Note that the tip angle α is a function of the scalar product $\int_0^{\tilde{\mathbf{r}}} \mathbf{G}_1 \cdot \mathrm{d}\tilde{\mathbf{r}}'$.

The maximum signal amplitude arises in the sample region for which the condition $\alpha = \psi$ is fulfilled. That is, the gradient vectors are parallel,

$$\mathbf{G_1} \| \mathbf{G_0}, \qquad [5]$$

[1] On leave from Department of Physics, Technical University, 3400 Cluj-Napoca, Romania. E-mail: ioan.ardelean@physik.uni-ulm.de.

1090-7807/00 $35.00

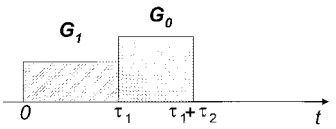

FIG. 1. Pulse sequence for the generation of the nutation echo. $\mathbf{G_1}$ and $\mathbf{G_0}$ are gradients of the RF amplitude $B_{1\perp}$ (component perpendicular to $\mathbf{B_0}$) and of the external magnetic flux density B_0, respectively.

and the magnitudes obey

$$G_1\tau_1 = G_0\tau_2. \qquad [6]$$

The region where these conditions are closely approached gives rise to localized nutation echo signals to be discussed in the following.

At low external magnetic fields B_0 or for short evolution times τ_2, that is, for $\xi \ll 1$, the influence of the demagnetizing field on the nutation echo can be neglected. In such circumstances and in the absence of relaxation and diffusion effects, half of the initial equilibrium magnetization is recovered,

$$m_{\max} = M_0/2, \qquad [7]$$

in analogy to the Hahn echo produced by two 90° RF pulses. Note that in the treatment given in Ref. (*4*), the phase direction of the RF pulse was assumed to be along the x axis of the rotating frame.

In the case where the gradients $\mathbf{G_1}$ and $\mathbf{G_0}$ are functions of the position, the nutation echo forms a localized signal suitable for volume-selective investigations. For example, such a situation arises with the (inhomogeneous) $\mathbf{B_1}$ field of a surface coil combined with a (constant) B_0 gradient generated with the gradient coils of a usual NMR imaging system. Figure 2 shows a schematic illustration of the two gradients acting at a position $\mathbf{r}$. From this position, a nutation echo signal arises if the conditions given in Eqs. [5] and [6] are fulfilled. Varying the magnitude or the duration of the gradient pulses and the direction of the B_0 gradient makes it possible to select the position where echo formation is to happen. Note that the appropriate superposition of B_0 gradient components along the three space directions of the laboratory frame results in a gradient in any desired direction. In this way, one can point to the volume of interest just as one does when shining with a torch to a keyhole in the dark, for instance. We therefore suggest to term this localization method "TORCH" (standing for "*t*apping *o*f *r*emote *coh*erences").

The spatial resolution with which the localized signals are generated and the shape of the selected volume element depend on how the gradients vary with position. For a discussion, let us consider the reduced density operator at the time $t = \tau_1 + \tau_2$ (see Fig. 1). An expression is given in Ref. (*4*, Eq. 22). Under the present assumptions and with the nomenclature used here, it reads

$$\sigma(\tau_1 + \tau_2) = [I_y\cos\psi + I_x\sin\psi]\sin\alpha + I_z\cos\alpha. \qquad [8]$$

Applying standard relations for trigonometric functions to Eq. [8] leads to terms like $\cos(\psi + \alpha)$ and $\cos(\psi - \alpha)$. Provided that strong enough gradients are applied, the term $\cos(\psi + \alpha)$ cannot give rise to any signal because its average over all positions within the sample cancels. This is in contrast to the $\cos(\psi - \alpha)$ term, the average of which, $\langle\cos(\psi - \alpha)\rangle$, is finite if $\psi = \alpha$. That is, echo signals selectively appear from regions of the sample volume V in which signals are superimposed more or less constructively so that

$$\langle\cos(\psi - \alpha)\rangle = \frac{1}{V}\int_V \cos(\psi - \alpha)\mathrm{d}V' \neq 0. \qquad [9]$$

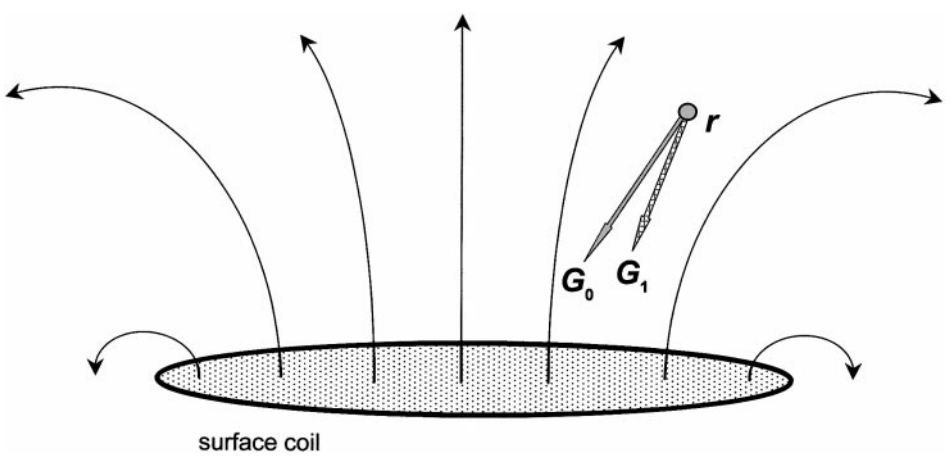

FIG. 2. Schematic representation of the RF field distribution of a surface coil. The generation of nutation echoes depends on how the local B_0 and $B_{1\perp}$ gradient vectors and their application intervals match.

The center of the selected volume, $\mathbf{r} = \tilde{\mathbf{r}}$, is located at the position where $\psi = \alpha$, that is, where the conditions given in Eqs. [5] and [6] are exactly fulfilled.

The dimension d of the sensitive volume can be estimated as follows. The angles α and ψ can be expressed in terms of the wavevectors, $\mathbf{k_1} = \gamma_n \tau_1 \mathbf{G_1}$ and $\mathbf{k_0} = \gamma_n \tau_2 \mathbf{G_0}$, respectively, so that the condition for a finite echo signal at a position $\tilde{\mathbf{r}}$ reads

$$\psi - \alpha = \int_0^{\tilde{\mathbf{r}}} (\mathbf{k_0} - \mathbf{k_1}) \cdot \mathrm{d}\tilde{\mathbf{r}}' \ll 2\pi. \qquad [10]$$

That is, the region in which the coherences are superimposed in a not completely destructive manner may roughly be characterized by the length

$$d \approx 2\pi / |\mathbf{k_0} - \mathbf{k_1}|_{\max}, \qquad [11]$$

where the subscript indicates the maximum deviation between the two wave vectors in the sensitive region to be detected. A combination of gradients with steep positional dependences leads to narrow localization, whereas flat positional variations broaden the region where signals are detected.

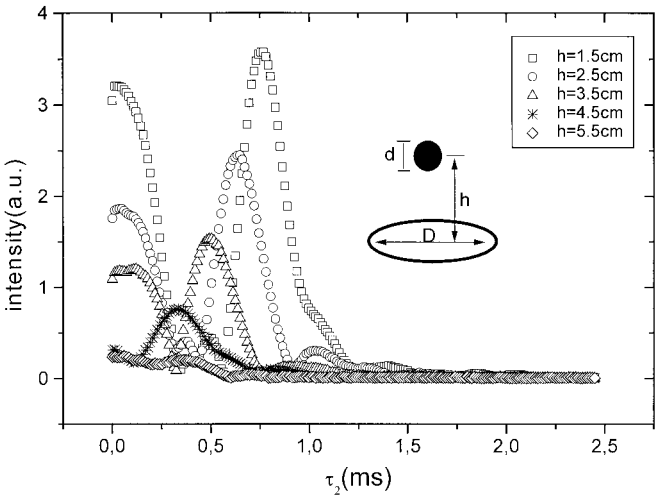

FIG. 3. Nutation echoes as a function of τ_2 (see Fig. 1). The sample was a spherical plastic container filled with water doped with $CuCl_2$. The outer diameter was $d = 2$ cm. The sphere was placed at varying heights h above the middle of a surface coil of diameter $D = 6$ cm as indicated. The probe was arranged in a 4.7-T tomography magnet. A constant gradient of the main field, $G_0 = 10$ mT/m, was applied along the RF coil axis. The height h of the sample above the surface coil was varied as indicated. The width of the radio frequency pulse was $\tau_1 = 3.1$ ms. The nutation echoes are well separated from the initial free-induction decays beginning at $\tau_2 = 0$ after the RF pulse.

3. EXPERIMENTS, SIMULATIONS, AND RESULTS

In order to demonstrate the spatial selectivity of the nutation echo, we have carried out three test experiments with different NMR spectrometers, RF coil geometries, and samples. Figure 3 shows the results obtained with a surface coil and a spherical sample of doped water placed at varying heights above the coil. The experimental details are given in the figure legend. A schematic representation of the sample arrangement is shown in the inset of Fig. 3. The nutation echo was recorded as a function of the interval τ_2 in a spatially constant and temporally steady gradient $\mathbf{G_0}$ for a given RF pulse width τ_1. That is, the matching condition in Eq. [6] is fulfilled at different positions for varying τ_2 values as a consequence of the gradient $\mathbf{G_1}(\mathbf{r})$ that increase with the distance before adopting a maximum value. The echoes consequently appear later for shorter spacings between the sphere and the RF coil.

The second test consists of mapping the spatial distribution of the transverse magnetization after forming the nutation echo. The pulse sequence used for this experiment is shown in Fig. 4. A conventional gradient-recalled echo imaging method (*10*) was employed, where the initial excitation RF pulse is replaced by the nutation echo sequence. Note that all B_0 gradients were spatially constant as before. Concerning the volume selection part, localization is therefore due to the distribution $\mathbf{G_1}(\mathbf{r})$ of the RF field gradient produced by the 6-cm surface coil.

A big water container was placed on the surface coil (see the schematic representation of dotted lines in Fig. 5). The "regions of interest" within this water container were selected by choosing different directions of the B_0 gradient in the τ_2 interval. The B_0 gradient direction was defined by correspondingly superimposing x and y gradients. The experimental results are displayed in Fig. 5. The volume selection effect is obvious. The regions where signals are visible is clearly shifted when turning the direction of the main field gradient. Note, however, that the localization properties of the TORCH experiment are much better than suggested by the images. Outside of the central region where the two nutation echo-forming gradients match according to Eqs. [5] and [6] and where the signal consequently is strongest, the sign of the signal contributions oscillates. Positive and negative contributions occur in different areas, depending on the local values of the phase angles α and ψ relative to each other. That is, most of the signal outside of the central gradient matching region cancels in volume selection experiments in which just the nutation echo induction signal is acquired. This is in contrast to the images that display the signal magnitude and, hence, positive and negative contributions equally. That is, the net signal provided by the nutation echo only represents the central region patterns displayed in the images.

In order to demonstrate this cancellation effect we have simulated the spatial distribution of the transverse magnetization using the MATHCAD software package. The same situation and the same parameters as in the experiments were assumed. The rotation induced by the local RF field on the local magnetization was calculated using a rotation matrix operator of the form (*11*)

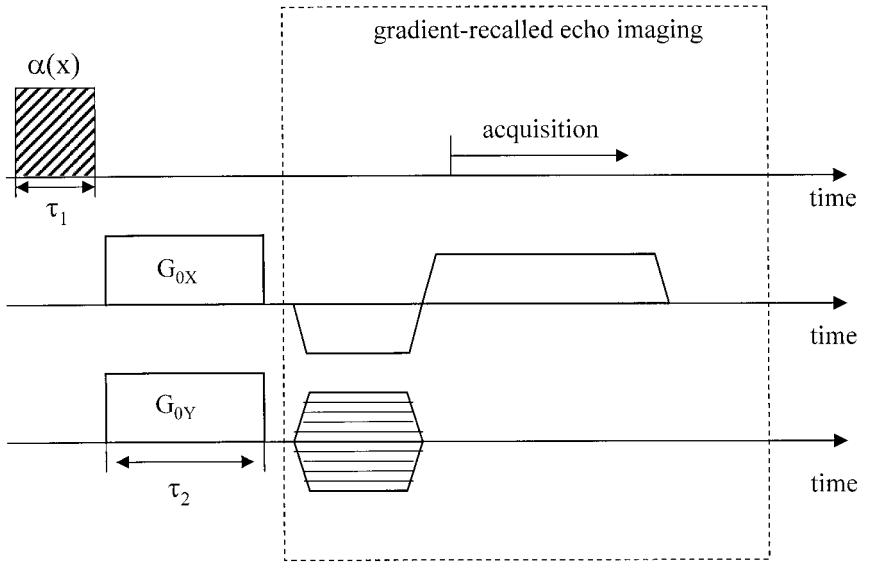

FIG. 4. Pulse sequence used for mapping the spatial distribution of the magnetization after generating a localized nutation echo. The RF pulse was produced with a 6-cm surface coil so that the RF field was inhomogeneously distributed in space. The tip angle, $\alpha(\mathbf{r})$, consequently was also a function of position. The local RF field is characterized by a gradient $\mathbf{G}_1(\mathbf{r})$. Spin coherences are refocused in a selected region by B_0 gradient pulses suitably matched to the B_1 gradient. The spatial distribution of the transverse magnetization produced in this way is mapped using an ordinary gradient-recalled echo imaging sequence.

$$R(\varphi) = \cos\frac{\varphi}{2} - 2i(pI_x + qI_y + rI_z)\sin\frac{\varphi}{2}. \qquad [12]$$

Here $\varphi(x, y, z) = ((\alpha_x(x, y, z))^2 + (\alpha_y(x, y, z))^2 + (\alpha_z(x, y, z))^2)^{1/2}$ represents the local rotation angle around the local RF field direction with the corresponding axial rotations $\alpha_j(x, y, z) = \gamma_n B_{1j}(x, y, z)\tau_1$ and $j = x, y, z$. The coefficients p, q, r in Eq. [12] are defined as $p(x, y, z) = \alpha_x(x, y, z)/\varphi(x, y, z)$, $q(x, y, z) = \alpha_y(x, y, z)/\varphi(x, y, z)$, and $r(x, y, z) = \alpha_z(x, y, z)/\varphi(x, y, z)$, respectively. The RF field distribution of the surface coil was calculated on the basis of Biot/Savart's law. Note that the above relation, Eq. [12], is valid only for $I = \frac{1}{2}$ spin quantum numbers and $p^2 + q^2 + r^2 = 1$.

Figure 6a shows the spatial distribution of the transverse magnetization in the central x, y plane. Apart from the absence of any "measuring sensitivity" limitation, this map closely corresponds to the experimental map shown in Fig. 5a. How-

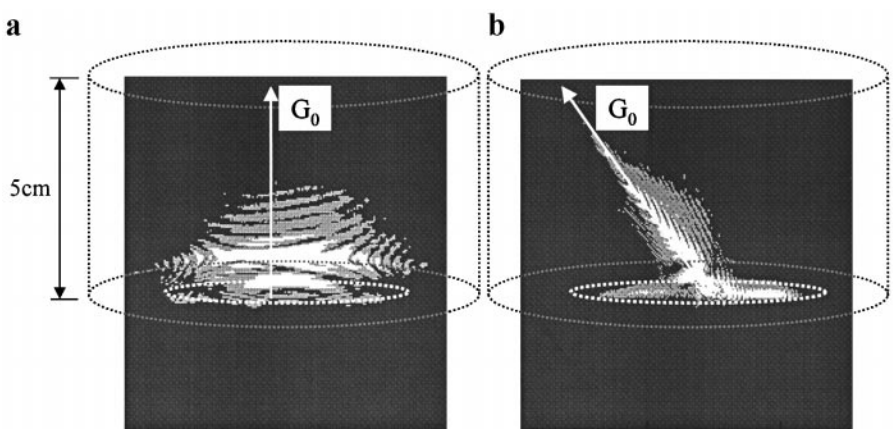

FIG. 5. Two-dimensional 4.7-T maps of the transverse magnetization following the nutation echo pulse sequence. The test sample was a cylinder of 7 cm radius filled up to a height of 5 cm with water doped with $CuCl_2$. The data were recorded using the pulse scheme shown in Fig. 4. The width of the radio frequency pulse was $\tau_1 = 4.9$ ms. The duration of the B_0 gradients employed for generating the nutation echoes was $\tau_2 = 1.5$ ms. The field of view is 8 cm × 8 cm corresponding to 256 × 256 pixels. The digital resolution is 310 μm. Map (a) was recorded with the nutation echo-forming B_0 gradient in the x direction (which is defined by the axis of the RF coil). The gradient strength was $G_{0x} = 7.5$ mT/m. In a second experiment represented by map (b) the direction of this gradient was generated by superimposing two gradients of strengths $G_{0x} = 7.5$ mT/m and $G_{0y} = 5$ mT/m, respectively. Note that the maps represent projections on the x, y plane. No slice selection is implied.

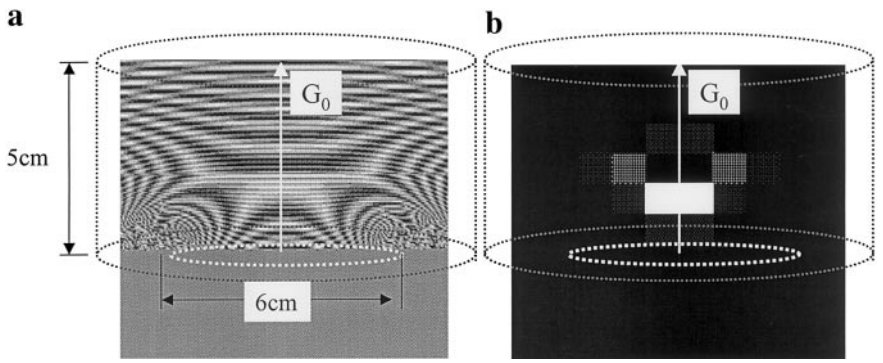

FIG. 6. Simulation of the distribution of the transverse magnetization in the central plane of the object Fig. 5 refers to. The RF field distribution of the surface coil was calculated on the basis of Biot/Savart's law. The current strength in the loop during the RF pulse was assumed to be $I = 2.8$ A. The RF pulse width was assumed to be $\tau_1 = 4.9$ ms. The refocusing gradient pulse of the main magnetic field was assumed along the x direction. Its strength and width was set to $G_0 = 7.5$ mT/m and $\tau_2 = 1.5$ ms, respectively, as in the real experiment. The simulation refers to a cubic object with 8 cm edge length divided into $200 \times 200 \times 200$ volume elements. Plot (a) shows the spatial distribution of the x magnetization in the central x, y plane (containing the coil axis). This transverse-magnetization map closely corresponds to the experimental image shown in Fig. 5a. Plot (b) shows the same data set as in (a) but now averaged into matrices of 10×10 macropixels. Contributions below the noise level typical in real experiments are suppressed. The white macropixels represent a mean signal strength about 3 times stronger than that of the next intense macropixels. The localization to be expected in TORCH experiments is obvious.

ever, unlike the experimental circumstances, we can now distinguish between positive and negative signal contributions. That is, we can take the cancellation effect into account by forming the average signal in more extended pixels.

The simulated transverse-magnetization map was subdivided into matrices of 10×10 "macropixels," in each of which the average signal contribution was calculated. The resulting distribution of the average transverse magnetization is shown in Fig. 6b. From these average signals all contributions below the typical noise level in real experiments are suppressed. Obviously most of the signal outside of the central region cancels. This result demonstrates that the TORCH experiment provides well-defined localized signals from the region around the position where exact matching according to Eqs. [5] and [6] is fulfilled.

A third test experiment was performed using a conic RF coil as described in Ref. (*5*). In this case a conventional Bruker DPX400 spectrometer without a B_0 gradient unit was employed. That is, the corresponding field gradient was produced by intentional misadjustment of the shimming currents. A test object consisting of two separate compartments filled with polydimethylsiloxane (PDMS) of molecular mass 17,000 was examined. A schematic representation of the arrangement is shown in the inset of Fig. 7. Experimental details are given in the legend to Fig. 7. Two echoes were observed due to the different gradient strengths experienced by the spins in the two compartments, that is, at different positions on the coil axis. The first echo, e1, corresponds to a smaller RF gradient than echo e2 and is, therefore, due to the more remote compartment. The echo amplitude consistently indicates that the detection sensitivity is also reduced at this position.

The appearance of a free-induction decay signal in Figs. 3 and 7 is due to an incomplete cancellation of the transverse magnetization following the RF gradient pulse. Although this residual signal can clearly be distinguished from the proper nutation echoes, its suppression might be desirable using more sophisticated coil designs.

The signal trains shown in Fig. 7 can be considered as one-dimensional reciprocal space images. Provided that the B_0 gradient is spatially constant, the Fourier transforms would represent one-dimensional real-space images, that is, projections on the B_0 gradient direction. The signals in Fig. 7 also suggest that the spatial resolution is affected by the duration of the RF gradient pulse.

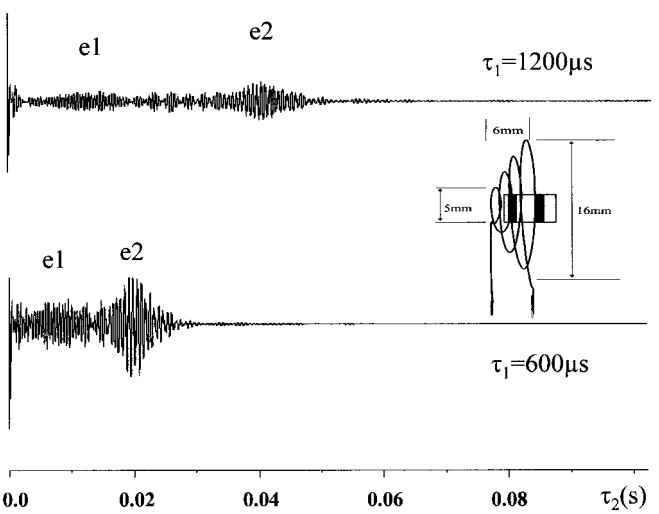

FIG. 7. Nutation echoes as a function of τ_2 (see Fig. 1). The sample was a two-compartment container filled with PDMS 17,000. The inset shows a schematic representation of the sample arrangement. The PDMS compartments (drawn in black) were 1.5 mm thick and had a spacing of 2.5 mm. The B_0 gradient was generated by the shimming system. The two compartments lead to two nutation echoes, e1 and e2, according to the different RF gradients acting at these positions. The signal trains were recorded for a width of the RF pulse of $\tau_1 = 600$ and 1200 μs, respectively.

4. CONCLUSIONS

In this paper we have described the nutation echo formed by a combination of pulsed gradients $B_{1\perp}$ and B_0. As an application we suggest the TORCH method, which is an easy-to-adjust technique for localized NMR provided that the spatial distribution of the field gradients is known. In the case of simple hardware geometries such as a surface coil placed in a tomography B_0 gradient system this information is readily available. We note also that $B_{1\perp}$ of any RF coil geometry can be probed experimentally by mapping the matching conditions, Eqs. [5] and [6], with a small test sample in a known constant B_0 gradient. Geometries of the RF coil other than those of this study might provide stronger RF field gradients (see, e.g., Ref. (*12*)). Also, the combination with nonuniform gradients of the main magnetic field promises a better spatial resolution. It should be noted that localized nutation echoes are expected to play a crucial role in applications such as the NMR MOUSE (*13*) or borehole NMR (*14*).

ACKNOWLEDGMENTS

This work has been supported by the Deutsche Forschungsgemeinschaft, the Volkswagen-Stiftung, and the Alexander von Humboldt Stiftung.

REFERENCES

1. A. L. Bloom, Nuclear induction in inhomogeneous fields, *Phys. Rev.* **98,** 1105 (1955).
2. R. Kaiser, The edge echo, *J. Magn. Reson.* **42,** 103 (1981).
3. A. Jerschow, Multiple echoes initiated by a single radio frequency pulse in NMR, *Chem. Phys. Lett.* **296,** 466 (1998).
4. R. Kimmich, I. Ardelean, Y.-Y. Lin, S. Ahn, and W. S. Warren, Multiple spin echo generation by gradients of the radio frequency amplitude: Two-dimensional nutation spectroscopy and multiple rotary echoes, *J. Chem. Phys.* **111,** 6501 (1999).
5. I. Ardelean, A. Scharfenecker, and R. Kimmich, Two-pulse nutation echoes generated by gradients of the radio frequency amplitude and of the main magnetic field, *J. Magn. Reson.* **144,** 45 (2000).
6. G. Deville, M. Bernier, and J. M. Delrieux, NMR multiple echoes observed in solid ^{3}He, *Phys. Rev. B* **19,** 5666 (1979).
7. D. Einzel, G. Eska, Y. Hirayoshi, T. Kopp, and P. Wölfle, Multiple spin echoes in a normal Fermi liquid, *Phys. Rev. Lett.* **53,** 2312 (1984).
8. W. Dürr, D. Hentschel, R. Ladebek, R. Oppelt, and A. Oppelt, Abstracts of the Society of Magnetic Resonance in Medicine, 8th Annual Meeting, Amsterdam, p. 1173, 1989.
9. R. Bowtell, R. M. Bowley, and P. Glover, Multiple echoes in liquids in a high magnetic field, *J. Magn. Reson.* **88,** 643 (1990).
10. R. Kimmich, "NMR Tomography, Diffusometry, Relaxometry," Springer-Verlag, Berlin (1997).
11. M. Goldman, "Quantum Description of High-Resolution NMR in Liquids," Clarendon Press, Oxford (1988).
12. K. Woelk, J. W. Rathke, and R. J. Klinger, Rotating-frame NMR microscopy using toroid cavity detectors, *J. Magn. Reson. A* **105,** 113 (1993).
13. B. Blümich, P. Blümler, G. Eidmann, A. Guthausen, R. Haken, U. Schmitz, K. Saito, and G. Zimmer, The NMR MOUSE: Construction, excitation, and applications, *Magn. Reson. Imaging* **16,** 479 (1998).
14. R. L. Kleinberg and C. Flaum, Review: "NMR Detection and Characterization of Hydrocarbons in Subsurface Earth Formations," *in* "Spatially Resolved Magnetic Resonance" (P. Blümler, P. Blümich, R. Botto, and E. Fukushima, Eds.), pp. 555–573, Wiley–VCH, Weinheim (1998).